Building and Environment 304 (2026) 115131

Contents lists available at ScienceDirect

Building and Environment

journal homepage: www.elsevier.com/locate/buildenv

Experimental assessment of the CO_2 phytoremediation efficiency of living walls in indoor environments

Gianluca Coccia [a,*], Feliciano Falcone [a], Luca Tarabelli [a], Costanzo Di Perna [a], Elisa Di Giuseppe [b], Marco D'Orazio [b]

[a] Marche Polytechnic University, Department of Industrial Engineering and Mathematical Sciences, Via Brecce Bianche 12, Ancona, 60131, Italy
[b] Marche Polytechnic University, Department of Construction, Civil Engineering and Architecture, Via Brecce Bianche 12, Ancona, 60131, Italy

HIGHLIGHTS

- Passive living walls measurably reduce indoor CO2 accumulation.
- CO2 removal increases with LED intensity and temperature.
- Full illumination cuts cumulative CO2 exposure by up to 44%.
- Pulse tests show CO2 reductions up to 39% under LEDs.
- Living walls can complement hybrid ventilation strategies.

ARTICLE INFO

Keywords:
Living wall
CO_2 mitigation
Indoor air quality
Phytoremediation
Climate chamber
Equivalent CO_2 removal airflow

ABSTRACT

Living walls (LWs) may complement conventional ventilation by mitigating indoor carbon dioxide (CO_2) accumulation. This study experimentally quantified the CO_2 phytoremediation performance of two passive LWs installed in a 38 m^3 full-scale climate chamber and composed of *Spathiphyllum*, *Philodendron hederaceum*, and *Epipremnum aureum*. Decay and pulse tests were performed at 20 °C and 24 °C under three lighting conditions: LED OFF, 50%, and 100% intensity. In the decay tests, illumination increased the measured decay constant k from 0.00566 min^{-1} to 0.00816 min^{-1} at 20 °C and 0.01105 min^{-1} at 24 °C, reducing cumulative CO_2 exposure by up to 44%. After subtraction of the OFF reference contribution, the net LW-equivalent CO_2 removal airflow rate was 5.75 m^3 h^{-1} at 20 °C and 12.39 m^3 h^{-1} at 24 °C. A concentration-dependent net uptake relationship, $g_{NET}(C)$, was also derived for use as a biological sink model. Pulse tests simulated the CO_2 generation of approximately three school-aged children. After 60 min, the final concentration increase ΔC was reduced by 20–27% and 35–39% at 20 °C under 50% and 100% LED intensity, respectively, and by 26–27% and 33–37% at 24 °C. Under full illumination, the equivalent respiratory load decreased from 3.3 to 2.1 occupants. Overall, passive LWs provided a measurable but limited CO_2 mitigation contribution and should be considered complementary biological sinks rather than substitutes for ventilation.

1. Introduction

Indoor air quality (IAQ) is closely linked to the physical and mental well-being of people in schools, offices, and other indoor environments [1]. Since people spend up to 90% of their time indoors, particularly during winter [2,3], inadequate ventilation may cause discomfort, headaches, irritation, and symptoms associated with Sick Building Syndrome, even when temperature and humidity remain within acceptable ranges [4–6].

IAQ is generally controlled through Controlled Mechanical Ventilation (CMV) and Heating, Ventilation and Air-Conditioning (HVAC) systems. However, high outdoor-air supply rates can substantially increase heating and cooling demand, especially in airtight buildings [7,8], whereas reducing ventilation may save energy at the

* Corresponding author.
Email addresses: g.coccia@staff.univpm.it (G. Coccia), f.falcone@pm.univpm.it (F. Falcone), l.tarabelli@pm.univpm.it (L. Tarabelli), c.diperna@staff.univpm.it (C. Di Perna), e.digiuseppe@staff.univpm.it (E. Di Giuseppe), m.dorazio@staff.univpm.it (M. D'Orazio).

https://doi.org/10.1016/j.buildenv.2026.115131
Received 17 June 2026; Received in revised form 23 July 2026; Accepted 14 August 2026
Available online 17 August 2026

Nomenclature

Latin symbols

A	Total one-sided leaf area of the two LWs (m^2)
A_{LW}	Total projected vegetated area of the Living Walls (m^2)
a, b	Regression coefficients (-)
C	CO_2 concentration (ppm)
C^*	Normalized CO_2 concentration; residual fraction in decay tests and relative concentration growth in pulse tests (%)
c_{le}	Light extinction coefficient (-)
c_{water}	Water vapour concentration (ppm)
ΔC	CO_2 concentration increase during pulse tests (ppm)
ΔQ	Difference between the net LW-equivalent CO_2 removal airflow rate and the design airflow rate ($m^3.h^{-1}$)
g	Leaf-area-normalized, system-level CO_2 uptake flux ($kg.m^{-2}.s^{-1}$)
K_{eff}	CO_2 removal coefficient ($m^3.min^{-1}$)
k	CO_2 decay constant (min^{-1})
LAI	Leaf Area Index (-)
M	Cumulative CO_2 exposure (ppm.min)
M_{CO_2}	Molar mass of CO_2 ($kg.mol^{-1}$)
n	Air change rate (h^{-1})
P	Atmospheric pressure (Pa)
PAR	Photosynthetically Active Radiation ($\mu mol\ m^{-2}\ s^{-1}$)
Q	Design airflow rate prescribed by EN 16,798–1 ($m^3.h^{-1}$)
R	Universal gas constant ($8.314 J.mol^{-1}.K^{-1}$)
t	Time (min)
t_d	Decay time (min)
$t_{1/2}$	Half-decay time (min)
T	Temperature (K, °C)
V	Chamber volume (m^3)

Greek symbols

β	Steepness parameter of the sigmoidal uptake model (-)
η	Phytoremediation efficiency (-)
θ	Normalized excess CO_2 concentration ratio (-)
τ	Optical transmittance (-)

Subscripts

∞	Asymptotic/background reference value
i	Inflection point of the sigmoidal model
max	Maximum
min	Minimum
NET	Net contribution
OFF	Lights-off condition
ON	Lights-on condition
OFF,max	Maximum value reached under lights-off conditions

Acronyms

CMV	Controlled Mechanical Ventilation
CO_2	Carbon dioxide
HVAC	Heating, Ventilation and Air Conditioning
IAQ	Indoor Air Quality
LED	Light Emitting Diode
LW	Living Wall
RH	Relative Humidity
VOC	Volatile Organic Compounds

expense of IAQ. Older systems may also respond poorly to changing occupancy and pollutant loads [9], with potentially significant health and economic consequences [10–12]. These limitations encourage complementary solutions capable of supporting conventional ventilation while reducing part of its energy demand [13,14].

Vegetated systems may complement HVAC as natural filtration devices [15]. Green Walls (GWs) include Green Facades (GFs), typically formed by outdoor climbing plants, and Living Walls (LWs) [16–20]. LWs can also be installed indoors to support pollutant removal and IAQ improvement [21,22]. They are classified as active or passive according to the presence of forced airflow [22,23]. Active systems convey polluted air through the substrate and root–microbe complex, whereas passive systems rely on diffusion and ambient air movement [24,25]. Although active LWs generally achieve higher removal rates, passive systems require no fan, generate less noise, and may be more suitable for continuously occupied spaces.

Previous studies associated LWs with improved indoor humidity, thermal comfort, IAQ, and reduced ventilation-related energy demand [20,26–30]. Lower CO_2 concentrations and fresh-air energy use were also reported, with peak CO_2 reductions approaching 50% [31,32]. In educational environments, LWs may additionally provide biophilic benefits, while classroom studies observed modest CO_2 reductions, improved thermal and humidity conditions, reduced stress, and better perceived air quality [33–35].

LW CO_2 removal depends on plant species [22,36], lighting conditions [16,37], foliage characteristics, and airflow configuration [30]. Species differ in photosynthetic activity, leaf area, and root-zone microbial interactions [38]. Commonly investigated species and their main removal mechanisms are summarized in Table 1. Supplementary lighting can enhance photosynthetic CO_2 uptake but also consumes electricity and generates heat; LW design must therefore balance removal performance against lighting-related energy use.

Despite the reported benefits, evidence on passive indoor LWs remains limited and fragmented. CO_2 removal rates are difficult to compare because standardized metrics are lacking, while information on long-term plant health, operational stability, life-cycle impacts, economic feasibility, and system design remains scarce. Moreover, many studies report only decay curves or test durations without deriving comparable engineering indicators. A reproducible quantitative framework is therefore needed to assess LW CO_2 removal performance. The present study addresses this gap through a full-scale experimental campaign conducted in a 38 m^3 climate chamber equipped with two LW panels, controlled irrigation, and adjustable lighting. Tests were performed at 20 °C and 24 °C with lights off and at 50% and 100% intensity. Decay tests assessed CO_2 removal after a controlled injection, while pulse tests simulated occupant-generated emissions. The concentration time series

Table 1
Most common plant species employed for VOC and CO_2 removal in indoor phytoremediation systems, with corresponding dominant mechanisms.

Species	Target pollutant	Main removal mechanism
Spathiphyllum wallisii (Peace Lily)	CO_2, VOCs [39–41]	Microbial biodegradation in rhizosphere
Dracaena deremensis	VOCs [42]	Root-zone microbial oxidation
Epipremnum aureum (Pothos)	CO_2, VOCs [42–45]	Photosynthesis and root microbial activity
Chlorophytum comosum (Spider Plant)	CO_2, VOCs [46]	Photosynthesis and rhizodegradation
Howea forsteriana (Kentia Palm)	CO_2 [38]	Photosynthetic uptake (large leaf area)
Dypsis lutescens (Areca Palm)	CO_2 [38,47]	Photosynthesis, low respiration loss
Chamaedorea elegans (Parlour Palm)	CO_2, VOCs [38,48]	Photosynthesis, moderate rhizosphere activity
Philodendron scandens	CO_2, VOCs, PM [38,49]	Adsorption on waxy leaf surfaces
Sansevieria trifasciata (Snake Plant)	CO_2, VOCs [46]	CAM photosynthesis (night CO_2 uptake)

were used to derive the decay constant k, half-decay time $\bar{t}_{1/2}$, cumulative exposure M, and net LW-equivalent CO_2 removal airflow rate $K_{plant,eff}$. These indicators provide a reproducible framework for comparing passive LW performance and supporting its future integration into hybrid ventilation strategies.

The paper is organized as follows. Sections 2 and Section 3 describe the experimental setup and methodological procedures. Section 4 presents and discusses the results of the study. Section 5 reports the conclusions.

2. Experimental setup

This section describes the climate chamber utilized for the experimental procedures, along with the LW used to evaluate CO_2 absorption and the measuring setup. The monitoring and control of these physical quantities were facilitated by the utilization of bespoke visualization interfaces (VIs) within the LabVIEW software framework.

2.1. Climate chamber

Experimental tests were conducted in a full-scale climate chamber measuring 4.3 × 3.3 × 2.7m (Fig. 1, internal volume of around 38m^3), located in the Environmental Energy Laboratory of the Department of Industrial Engineering and Mathematical Sciences (DIISM), Marche Polytechnic University, Ancona, Italy. The chamber consisted of a lattice-steel load-bearing frame enclosed by 0.45m-thick mineral-fibre insulating panels. The floor was made of medium-density fibre panels supported by a steel structure approximately 0.30m above the laboratory floor. Its dimensions correspond to approximately one quarter of a typical Italian classroom.

2.2. Living wall

Two fabric-based LW panels were installed on the east wall of the climate chamber. Each panel measured 1.35 × 2.35m and covered approximately 3.17m^2, giving a total projected vegetated area of 6.34m^2. The panels were supported by a metal frame and consisted of fabric pockets containing rock wool and natural fertilizer. Each panel was divided into upper and lower irrigation zones, while the irrigation system maintained the substrate moisture between 25 and 35%.

Fig. 2. Plant species and their distribution in the LWs. The left panel contains *Spathiphyllum* (Peace Lily), while the upper and lower sections of the right panel contain *Philodendron hederaceum* and *Epipremnum aureum* (Pothos), respectively.

Three species previously investigated for indoor phytoremediation were used (Fig. 2). The left panel was planted with *Spathiphyllum* [39–41], whereas the upper and lower sections of the right panel contained *Philodendron hederaceum* [38] and *Epipremnum aureum* [43–45], respectively.

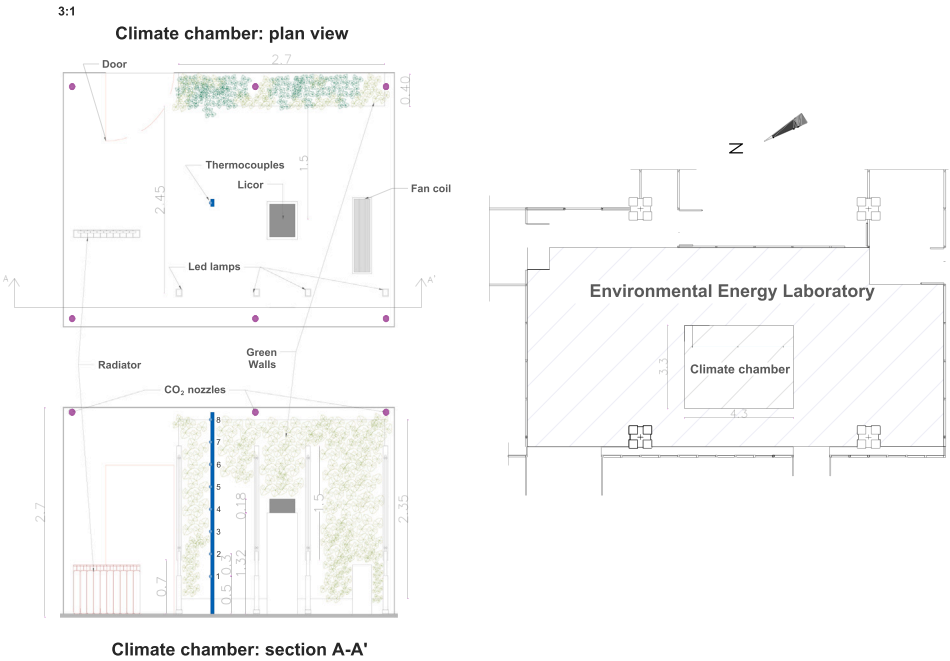

Fig. 1. Plan view and cross section of the full-scale climate chamber. All dimensions are provided in meters.

2.3. Measuring system

This section contains information on the monitoring techniques utilized in the present study. The analysis focuses on the following parameters: temperature, illumination, air humidity, and carbon dioxide concentration.

2.3.1. Lighting and leaf area index measurements

Four LED lamps were installed inside the climate chamber to provide the light required for plant maintenance and photosynthetic activity. Each lamp measured 1.5 × 0.7 × 0.4m, had a nominal electrical power of 125W, and provided a nominal photon flux of 250 μmol s^{-1} within the 400–700nm spectral range. As shown in Fig. 1, the lamps were positioned 2.45m from the LW supports, with their bases 0.70m above the floor and tilted upward by approximately 15° from the vertical.

A dedicated LabVIEW routine controlled the light intensity and the light–dark cycle. The default maintenance cycle consisted of 8 h of light and 16 h of darkness, while the LED intensity was adjusted according to the experimental conditions.

The spatial distribution of Photosynthetically Active Radiation (PAR) was measured 0.10m in front of the LWs using a Danoplus DP-380 portable quantum sensor operating in the 400–700nm range, with an instrumental accuracy of 1 μmol m^{-2} s^{-1} [50]. Measurements were taken over a 2.70 × 2.35m vertical plane divided into a 4 × 4 grid. The value assigned to each cell was the average of four measurements taken at its corners.

As shown in Fig. 3(a), at 50% LED power the measured PAR ranged from 40 to 61 μmol m^{-2} s^{-1}, with lower values near the lateral and lower boundaries. At full LED power (Fig. 3b), PAR ranged from 70 to 107 μmol m^{-2} s^{-1} and showed a more uniform distribution over the planting surface.

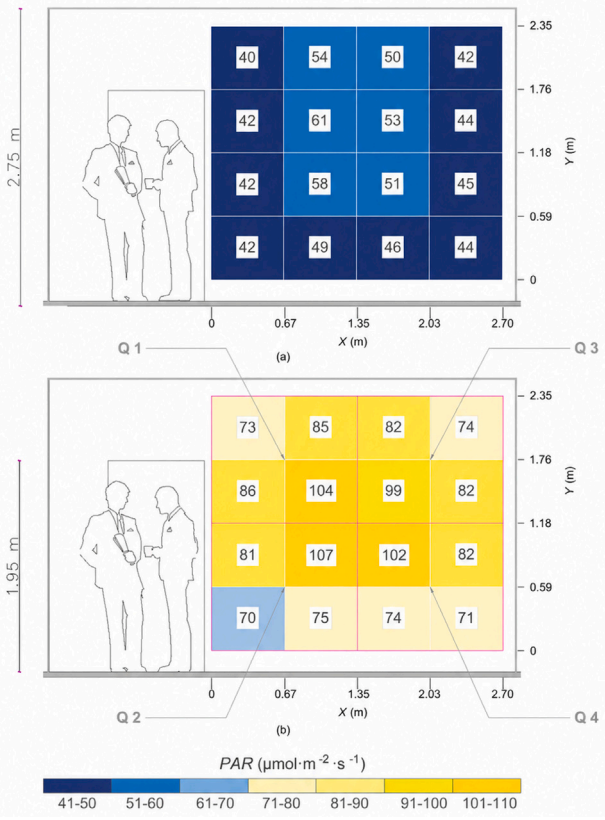

Fig. 3. PAR distribution in front of the LWs under two lighting conditions: (a) LED lamps at 50% power and (b) LED lamps at 100% power. The values represent the averages of four measurements taken at the corners of each grid cell.

Table 2
Measured PAR and calculated LAI for each quadrant.

Quadrant	Above PAR (μmol m^{-2} s^{-1})	Below PAR (μmol m^{-2} s^{-1})	τ	LAI
Q_1	87.0	28.1	0.32	1.42
Q_2	83.2	29.5	0.35	1.31
Q_3	84.2	29.7	0.35	1.31
Q_4	82.2	30.0	0.36	1.27

The PAR measurements were also used to estimate the Leaf Area Index (LAI), defined as the one-sided leaf area per unit projected area [51–54]. For this purpose, the LWs were divided into four sectors, Q_1–Q_4, as indicated in Fig. 3(b) (Q_1 and Q_2: *Spathiphyllum*; Q_3 and Q_4: *Philodendron hederaceum* and *Epipremnum aureum*). An indirect optical method based on PAR transmittance was adopted [52,55,56]. Measurements were taken immediately in front of and behind the foliage, and the optical transmittance τ was calculated as [57]:

$$\tau = \frac{\text{Average Below } PAR}{\text{Average Above } PAR} \tag{1}$$

Assuming a uniform leaf distribution and diffuse radiation conditions, LAI was calculated using the simplified Beer–Lambert law:

$$LAI = -\frac{\ln(\tau)}{c_{le}} \tag{2}$$

where c_{le} is the light extinction coefficient, which depends on foliage geometry and measurement conditions [52,55]. A value of $c_{le} = 0.8$ was adopted for the present laboratory configuration.

As reported in Table 2, the calculated LAI values ranged from 1.27 to 1.42, with differences below 10% among the four sectors. The mean value, equal to 1.3, was therefore adopted for the entire LW system and assumed constant during the experimental campaign, since foliage variations over the test period were considered negligible.

2.3.2. Temperature monitoring and control

Air temperature was measured every 10 s using eight copper–constantan T-type thermocouples with an uncertainty of 0.5 °C. As shown in Fig. 1, the sensors were arranged vertically on a pole located approximately 2m from the east wall containing the LWs. The lowest thermocouple was positioned 0.5m above the floor, and the remaining sensors were spaced at 0.3m intervals.

The mean value measured by the eight thermocouples was used as the reference temperature for the control system. An electric radiator and a fan coil unit, regulated through a PID controller and a dedicated LabVIEW virtual instrument, maintained the selected temperature set-point within ±0.5 °C throughout the experiments.

2.3.3. CO_2 concentration and air humidity measurements

A LI-COR LI-7815 Trace Gas Analyzer was used to measure the CO_2 concentration C and water-vapour concentration c_{water} at 1Hz, with measurement uncertainties of 0.1ppm and 45ppm, respectively. Relative humidity (RH) was derived from c_{water}. As shown in Fig. 1, the analyzer was positioned between the two LWs, approximately 1.5m from each panel and 1.5m above the floor.

CO_2 with a purity of 99.7% was supplied from an external cylinder through six ceiling-level nozzles symmetrically distributed along the two sides of the chamber, as shown in Fig. 1. Gas delivery was regulated by a solenoid valve controlled through a dedicated LabVIEW virtual instrument.

Before the installation of the LWs, the spatial distribution of CO_2 within the chamber was assessed using seven HOBO MX CO_2 Logger (MX1102 A) sensors, with a nominal accuracy of ±50*ppm*. The sensors were installed on three vertical poles located near the LWs, in the central region of the chamber, and on the opposite side. Sensors A and B were

Table 3
Average CO_2 concentration C (ppm) measured by the seven monitoring sensors during a preliminary decay test.

t	C (ppm)							Std. dev.
(min)	A	B	C	D	E	F	G	(ppm)
0	3049.3	3012.6	3055.1	3021.5	3029.5	3029.9	3030.5	14.9
20	2517.9	2476.8	2523.7	2488.7	2496.7	2499.0	2498.7	16.1
46	2009.5	1977.3	2020.2	1991.3	1997.8	1995.8	2002.6	13.6
94	1507.0	1478.2	1524.6	1494.9	1502.6	1498.4	1499.9	13.9
178	1003.2	976.7	1020.6	995.6	1007.2	999.9	1002.3	13.2
232	756.2	719.6	759.1	741.6	758.5	750.5	750.8	13.9
526	500.3	471.8	501.8	502.7	510.2	503.7	510.7	13.1
1030	389.5	374.5	391.7	407.5	408.5	412.9	415.5	15.1

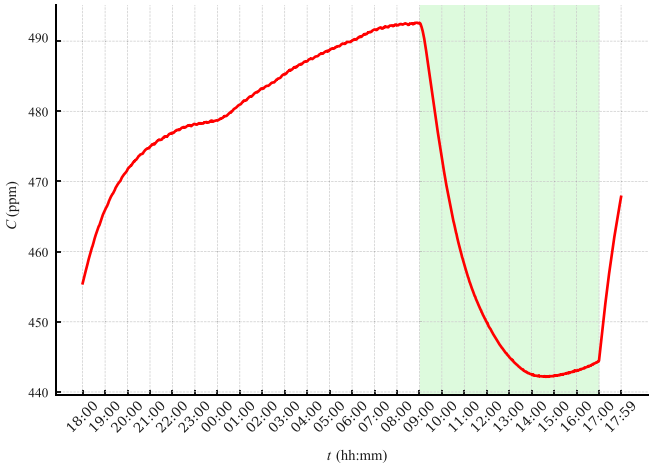

Fig. 4. Temporal evolution of CO_2 concentration C over one day in the test chamber with the door constantly closed. The green area highlights the period during which the lights were turned on. (For interpretation of the references to colour in this figure legend, the reader is referred to the web version of this article.)

positioned near the LWs at heights of 0.30 and 2.10m; sensors C–E were positioned in the central region at 0.30, 1.10, and 2.10m; and sensors F and G were positioned on the opposite side at 0.30 and 2.10m. These preliminary measurements were also used to optimize the nozzle positions and distribution-duct lengths, thereby limiting horizontal concentration differences and vertical stratification. As reported in Table 3, the spatial standard deviation among the seven monitoring points ranged from 13.1 to 16.1ppm, below the nominal sensor accuracy. No marked or persistent horizontal or vertical concentration gradients were observed. The results therefore indicated an approximately uniform CO_2 distribution and supported the use of the LI-COR measurement as representative of the mean chamber concentration.

Daily CO_2 monitoring was also performed with the chamber door closed to minimize air exchange with the surrounding laboratory. As shown in Fig. 4, during the dark period (18:00–08:59), C increased from 455.5 to 492.6ppm, corresponding to an average emission rate of 2.47ppm.h^{-1}. During the illuminated period (09:00–16:59), the concentration decreased to 444.4ppm, indicating that photosynthetic uptake exceeded respiratory CO_2 release. This daily carbon-exchange pattern is consistent with previous studies [11,37,58].

3. Methodology

This section presents the theoretical framework and experimental procedures adopted for the decay and pulse tests, following the tracer-gas methods described by [7] and commonly used to characterize LWs [59,60]. In decay tests, CO_2 was injected to establish a uniform initial concentration, and its subsequent decrease was monitored. In pulse tests, controlled CO_2 injections reproduced a continuous internal source, and the resulting concentration increase was recorded.

3.1. Decay method

The decay method was applied under the assumptions of a well-mixed chamber volume and spatially uniform mean air temperature (Section 2.3.3 and Table 3) [61]. Based on this preliminary assessment, the CO_2 concentration measured by the LI-COR analyzer was used as representative of the mean concentration within the climate chamber.

During the decay tests, the chamber remained closed, with no intentional supply or exhaust airflow and no further CO_2 injection. The observed decrease in CO_2 concentration resulted from the combined effects of plant-related CO_2 exchange and residual air leakage. Since these contributions could not be independently quantified, the overall removal process was represented by an effective first-order decay model [7,62,63]:

$$V \frac{dC}{dt} = -K_{eff}(C - C_\infty) \tag{3}$$

where V is the chamber volume, C is the absolute indoor CO_2 concentration, C_∞ is the asymptotic equilibrium concentration, and K_{eff} is an effective removal coefficient accounting for all relevant CO_2 removal and exchange processes. Defining

$$k = \frac{K_{eff}}{V} \tag{4}$$

integration of Eq. (3) yields:

$$\ln\left[\frac{C(t) - C_\infty}{C(0) - C_\infty}\right] = \ln(\theta) = -k\,t \tag{5}$$

where $C(0)$ is the initial concentration (3000ppm). The asymptotic concentration C_∞ was fixed at 500ppm, representing a controlled indoor background level under quasi-closed conditions, slightly above typical outdoor concentrations. If k_{ON} and k_{OFF} denote the corresponding decay constants measured with the LED lamps switched on and off, respectively, then the quantity:

$$K_{plant,eff} = V(k_{ON} - k_{OFF}) \tag{6}$$

can be interpreted as an equivalent CO_2 removal airflow rate (m^3.h^{-1}). This is not an actual airflow rate, but rather a theoretical one that, through air exchange with an environment at concentration C_∞, would produce the same CO_2 removal effect as the LW.

In addition to the logarithmic form used for the regression analysis, the same normalized concentration term was expressed as a residual fraction:

$$C^* = \frac{C(t) - C_\infty}{C(0) - C_\infty} \cdot 100 \tag{7}$$

The parameter C^* represents the percentage of the initial concentration excess that is still present in the chamber at time t, or equivalently the percentage of the decay path still to be completed before reaching the asymptotic concentration C_∞. Therefore, $C^* = 100\%$ at the beginning of the decay test and progressively decreases towards 0% as $C(t)$ approaches C_∞. This formulation is adopted because the decay process follows an exponential law; therefore, applying the logarithmic transformation yields a linear trend over the decay region, enabling the estimation of the decay coefficient k through regression on the linear portion of the curve [64]. Deviations from linearity, typically observed as a “knee” in the curve, indicate the transition towards the asymptotic regime.

Before each decay test, CO_2 was injected until a target concentration of 3000ppm was reached. The required mass of CO_2 was estimated from the ideal gas law using chamber volume, temperature and pressure. Approximately 200g of CO_2 was needed to raise the concentration from

500ppm to 3000ppm in the 38m^3 chamber, consistent with theoretical expectations. Injection proceeded in 30s pulses separated by 90s pauses, each pulse increasing the indoor concentration by about 200ppm, corresponding to an average mass flow rate of roughly 0.48g.s^{-1}. A decay test was considered complete when the indoor concentration returned to 500ppm; the corresponding elapsed time is denoted as the decay time t_d. Each test was repeated 3 times to assess repeatability and to evaluate the influence of the LW by comparing the lights-off and lights-on conditions.

To quantify cumulative CO_2 exposure during decay, the area under the curve M (ppm.min) was computed using the trapezoidal rule [7,65,66]:

$$M = \int_0^{t_d} C(t)\,dt \approx \frac{\Delta t}{2}\left(C_0 + 2C_1 + \cdots + 2C_{N-2} + C_{N-1}\right) \tag{8}$$

where Δt is the time interval between consecutive concentration samples and N is the total number of samples considered over the decay test. This parameter provides an integrated measure of exposure, overcoming the limitations of point-based indicators such as instantaneous concentration values. A dimensionless efficiency parameter was then defined as:

$$\eta = \frac{M_{OFF} - M_{LW}}{M_{OFF}} \tag{9}$$

where M_{OFF} and M_{LW} denote the cumulative exposure under lights-off and illuminated LW conditions, respectively. The parameter η represents the relative reduction in total CO_2 exposure and provides an integrated measure of the system performance.

The experimental decay curves, in which the indoor CO_2 concentration is expressed as a function of time $C = f(t)$, were processed to derive a concentration-dependent uptake relationship for the Living Wall (LW), namely $g = f(C)$. Expressing the uptake as a function of CO_2 concentration allows the LW to be represented as a dynamic sink, rather than describing its performance only through the duration of a specific decay test. This approach is consistent with plant-uptake models in which CO_2 removal depends on both ambient concentration and the amount of vegetation [67]. The resulting quantity should be interpreted as a system-level uptake flux derived from the CO_2 mass balance of the whole LW–chamber system, rather than as a direct measurement of leaf photosynthesis. It therefore reflects the combined response of the vegetation, canopy structure, substrate and experimental conditions.

The CO_2 concentration was originally acquired by the LI-COR analyzer at a frequency of 1 Hz and subsequently averaged over consecutive non-overlapping one-minute intervals, thus obtaining one mean concentration value per minute. The local rate of change of CO_2 concentration was estimated using a moving-window linear regression applied to the experimental data. Specifically, a least-squares linear regression was applied to five consecutive one-minute mean values. Each window therefore included five points, covering a 4 min interval between the first and last timestamps, and was shifted forward by one minute at each step. For each time instant, a subset of adjacent points was fitted through a least-squares approach, providing a local approximation of the form $C(t) = a\,t + b$, from which the slope dC/dt was obtained. This procedure provides a local estimate of the temporal derivative while reducing the influence of measurement noise. The five-point window was selected as a compromise between limiting short-term concentration fluctuations and preserving the local shape of the decay curve. Shorter windows would produce noisier derivative estimates, whereas wider windows would excessively smooth the concentration profile.

The local slopes, expressed in ppm.min^{-1}, were converted into a CO_2 mass flux per unit one-sided leaf area, $g_j(C)$ (kg.s^{-1}.m_{leaf}^{-2}), using the ideal gas law:

$$g_j(C) = -10^{-6}\,\frac{dC_j}{dt}\left(\frac{P\,V}{60\,R\,T\,A}\right)M_{CO_2}, \qquad j \in \{ON, OFF\} \tag{10}$$

Here, P is the atmospheric pressure, V is the chamber volume, R is the universal gas constant, T is the air temperature, and M_{CO_2} is the molar mass of CO_2. The factors 10^{-6} and 60 account for unit conversions, and the negative sign ensures that a concentration decrease corresponds to a positive uptake. The surface A represents the total one-sided leaf area of the two LW panels and was estimated as $A = LAI \cdot A_{LW}$, where A_{LW} is the total projected vegetated area and LAI is the experimentally determined Leaf Area Index. Leaf-area normalization is consistent with gas-exchange studies reporting CO_2 assimilation per unit leaf area [68] and with chamber experiments in which whole-plant CO_2 removal is normalized by the total leaf area [69]. In addition, LAI and foliage density are recognized as relevant factors affecting the carbon-sequestration performance of vegetated systems [70]. Using the total leaf area reduces the influence of the amount of foliage installed per unit wall area on the reported flux. Nevertheless, because the flux was obtained from the mass balance of the whole chamber and the leaf area was estimated through LAI, $g_j(C)$ remains an effective system-level parameter rather than a direct physiological measurement on individual leaves.

To improve robustness, the resulting $g_j(C)$ data were grouped into overlapping concentration bins, from which mean values and standard deviations were computed. The net uptake flux was then defined as:

$$g_{NET}(C) = g_{ON}(C) - g_{OFF}(C) \tag{11}$$

This subtraction isolates the additional CO_2 removal observed under illuminated conditions by accounting for the reference decay measured with the lighting system switched off. It therefore reduces the influence of background effects such as residual air exchange, mixing, sensor fluctuations and non-photosynthetic contributions. The relationship between CO_2 concentration and net uptake flux was then modeled using a sigmoidal function:

$$g_{NET}(C) = g_{min} + \frac{g_{max} - g_{min}}{1 + \exp[-\beta(C - C_i)]} \tag{12}$$

In this formulation, g_{min} and g_{max} are the lower and upper asymptotic uptake fluxes, respectively. The parameter C_i is the inflection concentration, at which $g_{NET} = (g_{min} + g_{max})/2$, while β describes the steepness of the transition around C_i. The sigmoidal function provides a bounded empirical description of the observed increase in CO_2 uptake with concentration and its gradual approach to an upper value at higher concentrations. It should therefore be regarded as a model of the tested LW under the investigated lighting, temperature, irrigation and canopy conditions, rather than as a universal law of plant photosynthesis. Its use outside the experimental concentration range or for LWs with substantially different characteristics requires additional validation.

A weighted regression was adopted to account for data heteroskedasticity, assigning weights inversely proportional to the variance. Parameter uncertainty was finally assessed through a non-parametric bootstrap approach, enabling the estimation of confidence intervals.

3.2. Pulse technique

Pulse tests were performed at 20 °C and 24 °C under three lighting conditions: lights off, 50%, and 100%, corresponding to the configurations described in Section 2.3.1 and shown in Fig. 3(a) and (b). As in the decay tests described in Section 3.1, each condition was repeated three times to assess repeatability.

The tests simulated a dynamic indoor scenario in which occupants continuously generate CO_2. According to EN 16798-1:2019 [71], the reference occupancy density for primary and secondary classrooms is 0.52persons/m^2, corresponding to approximately seven students in the 14 m^2 chamber. A reduced occupancy of three children was considered in the present study.

The CO_2 generation rate was calculated using the method proposed by [72], which accounts for basal metabolic rate and activity level rather than relying solely on simplified tabulated values [73–75]. For children

aged 6–11 years performing light activity (1.3met [76]), linear interpolation between the generation rates reported at 1.2met and 1.4met gives 0.00325 L s^{-1} (0.195 L min^{-1}) per child. The resulting rate for three children is 0.585 L min^{-1}, equivalent to a theoretical increase of approximately 150ppm in 10 min within the 38 m^3 chamber in the absence of removal processes. This emission rate was reproduced by setting the discharge pressure to 2bar and controlling the solenoid valve through a LabVIEW routine, which opened the valve for 1 s every 60 s. Each test lasted 60 min. This duration was selected a priori to represent a one-hour classroom occupancy period and was applied consistently to all OFF and ON tests. Because the CO_2 concentration was still increasing at the end of the tests, the experiments describe transient accumulation over a fixed observation period rather than steady-state conditions. The reported percentage reductions therefore compare the CO_2 accumulation measured at $t = 60$ min under ON conditions with the corresponding OFF condition.

From a mass-balance perspective, the measured concentration profile reflects the balance between continuous internal CO_2 generation and removal through natural air exchange and LW uptake. Assuming that background air exchange remained unchanged between OFF and ON tests, the difference between their concentration profiles was attributed to the net contribution of the LW.

Because the initial CO_2 concentration varied slightly among repetitions, the curves were normalized before comparison. In the decay tests, C^* represents the residual fraction of the concentration decrease from 3000ppm to 500ppm; in the pulse tests, it represents the relative concentration increase with respect to the corresponding OFF condition. The lower reference concentration was set to $C_\infty = 500ppm$, consistent with the decay analysis, while the upper reference was $C_{\mathrm{OFF,max}}$:

$$C^* = \frac{C(t) - C_\infty}{C_{\mathrm{OFF,max}} - C_\infty} \cdot 100 \tag{13}$$

Here, $C_{\mathrm{OFF,max}}$ is the concentration measured at $t = 60$ min during the corresponding lights-off test. Since the OFF profiles were still increasing at that time, this value represents the endpoint of the observation period rather than an equilibrium concentration. Accordingly, $C^* = 0\%$ represents the background concentration and $C^* = 100\%$ the OFF endpoint. Lower final values under ON conditions indicate reduced CO_2 accumulation over the same observation period.

4. Results and discussion

This section collects and describes the results obtained during the experimental campaign, first analyzing and discussing the decay-type tests and then the pulse-type tests.

4.1. Decay tests

The decay tests were performed with the LED lamps switched off and under full illumination (LED 100%, average incident PAR of 90 μmol m^{-2} s^{-1}) at two temperature set-points, namely 20 °C and 24 °C. While the OFF tests provided the reference decay in the absence of photosynthetic activity which includes residual air exchange and other background effects, the comparison between the two illuminated conditions was used to assess the influence of temperature on the CO_2 removal performance of the system.

Fig. 5(a) shows the linearized concentration profiles as $\ln(\theta)$, whose slopes determine the decay constants k, while Fig. 5(b) reports the corresponding $C(t)$ and $C^*(t)$ profiles. The experimental profiles follow the expected exponential behavior described by the mass-balance model in Section 3.1.

Illumination clearly accelerated the CO_2 decay compared with the OFF condition. After 60 min, the average concentration decreased to 2202.5ppm under OFF conditions, compared with 1878.4ppm at 20 °C and 1819.6ppm at 24 °C; the corresponding normalized values were $C^* = 68.1\%$, 55.1%, and 52.8%, respectively. The difference persisted throughout the tests: after 180 min, the concentrations were 1325.6ppm, 990.4ppm, and 872.8ppm, respectively. These results show that the illuminated LW enhanced CO_2 removal, with the fastest decay observed at 24 °C.

The limited variation among the three repetitions indicates good experimental repeatability under all investigated conditions (Table 4). The mean decay constant was 0.00566 min^{-1} under OFF conditions and increased to 0.00816 min^{-1} at 20 °C and 0.01105 min^{-1} at 24 °C when

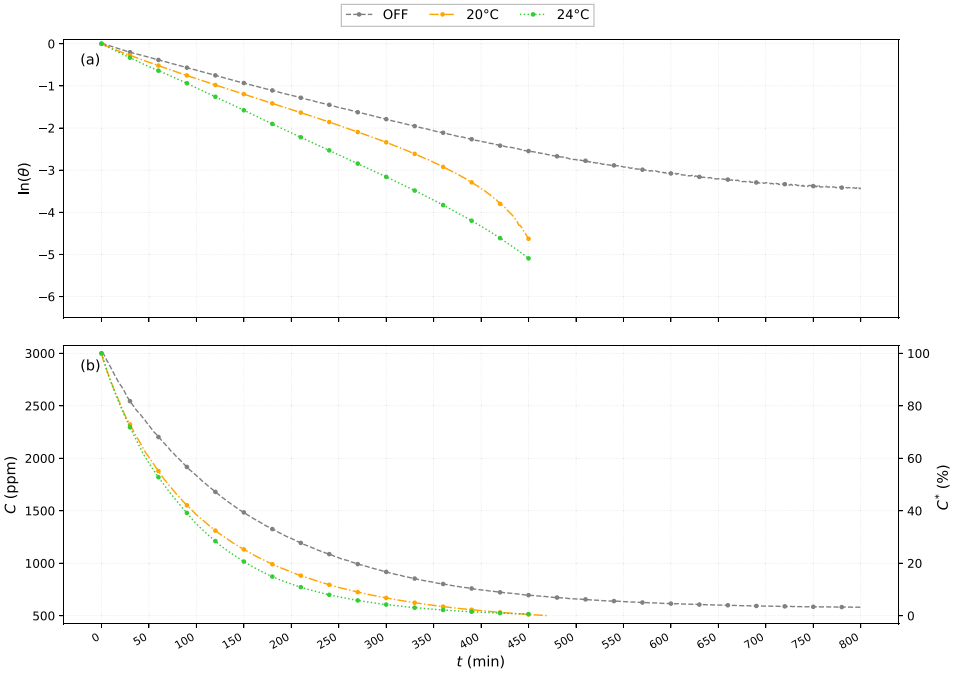

Fig. 5. Average decay curves of indoor CO_2 concentration under the investigated experimental conditions. Panel (a) shows the linearized variable $\ln(\theta)$ according to Eq. (5). Panel (b) presents the corresponding CO_2 concentration $C(t)$ in ppm.

Table 4
Summary of decay constants, integral quantities, and net phytoremediation indicators for each investigated condition.

Condition	k (min^{-1})				$\bar{t}_{1/2}$	M	η
	Test 1	Test 2	Test 3	$\bar{k}$	(min)	(ppm.min)	(-)
OFF	0.00562	0.00566	0.00570	0.00566	122	824,195	
ON 20 °C	0.00814	0.00816	0.00818	0.00816	85	497,752	0.396
ON 24 °C	0.01103	0.01105	0.01107	0.01105	63	458,568	0.444

Table 5
Comparison between the design airflow rates prescribed by EN 16,798–1 and the net LW-equivalent CO_2 removal airflow rates under illuminated conditions. Negative ΔQ values indicate that the LW-equivalent contribution is lower than the corresponding design airflow requirement.

Occupants	Category	$Q(m^3.h^{-1})$	$n(h^{-1})$	$\Delta Q_{20}(m^3.h^{-1})$	$\Delta Q_{24}(m^3.h^{-1})$
1	III	35.6	0.93	-29.9	-23.2
1	II	47.1	1.23	-41.4	-34.7
1	I	59.2	1.54	-53.5	-46.8
2	III	51.8	1.35	-46.1	-39.4
2	II	68.7	1.79	-63.0	-56.3
2	I	86.2	2.25	-80.5	-73.8
3	III	68.0	1.78	-62.3	-55.6
3	II	90.3	2.36	-84.6	-77.9
3	I	113.2	2.95	-107.5	-100.8
4	III	84.2	2.20	-78.5	-71.8
4	II	111.9	2.92	-106.2	-99.5
4	I	140.2	3.66	-134.5	-127.8

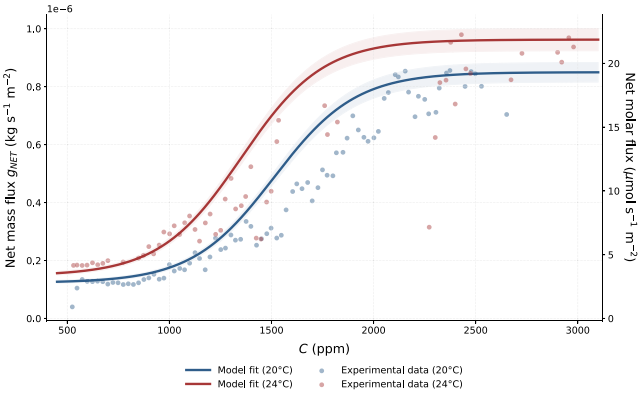

Fig. 6. Comparison between experimental data and the fitted model of the net CO_2 uptake flux g_{NET} as a function of indoor CO_2 concentration C under the two investigated thermal conditions (20 °C and 24 °C).

Table 6
Fitted parameters of the sigmoidal model describing the net CO_2 uptake flux g_{NET} as a function of concentration for the investigated temperature conditions.

T (°C)	g_{min} (kg.m^{-2}.s^{-1})	g_{max} (kg.m^{-2}.s^{-1})	β	C_i (ppm)
20	1.23e-7	8.48e-7	0.0049	1510
24	1.50e-7	9.63e-7	0.0049	1352

the LED lamps were switched on. The deviation between the ON and OFF conditions, proportional to the net LW contribution, was around 31% at 20 °C and 49% at 24 °C. The same trend was reflected in the other performance indicators, as reported in Table 4. Overall, these indicators consistently show that illumination enhanced the CO_2 removal process, with a stronger net effect at 24 °C.

Table 5 reports the airflow rates Q and air change rates n prescribed by EN 16,798–1 for different occupancy levels and IAQ categories. According to Eq. (6), the net LW-equivalent CO_2 removal airflow rate was 5.75 m^3 h^{-1} at 20 °C and 12.39 m^3 h^{-1} at 24 °C. For each configuration, ΔQ_{20} and ΔQ_{24} in Table 5 represent the difference between the net LW-equivalent CO_2 removal airflow rate and the corresponding EN 16,798–1 design requirement. The negative values obtained in all configurations indicate that the net contribution of the LW remained always lower than the airflow prescribed by the standard. The deficit increases with both occupancy and required IAQ category because the prescribed outdoor airflow increases, whereas the LW-equivalent contribution remains constant for the tested configuration. The LW should therefore be regarded as a complementary biological sink rather than as a standalone substitute for natural or mechanical ventilation. In this context, the equivalent airflow is intended as an engineering performance indicator that quantifies the additional CO_2 removal provided by the LW; it does not represent an actual outdoor airflow and does not imply that the LW can replace the ventilation rates prescribed by the standard.

Fig. 6 and Table 6 show that the net uptake flux g_{NET} (Eq. 12) increased nonlinearly with indoor CO_2 concentration and gradually approached an upper plateau. The adopted sigmoidal model reproduced this concentration-dependent behavior under both temperature conditions. The comparison between the two fitted curves shows that the LW exhibited a greater net CO_2 uptake capacity at 24 °C. This difference is reflected in the upper asymptotic flux g_{max}, which increased from 8.48×10^{-7} to 9.63×10^{-7} $kg.m^{-2}.s^{-1}$, and in the characteristic concentration C_i, which decreased from 1510ppm to 1352ppm. The lower asymptotic flux g_{min} was also slightly higher at 24 °C, increasing from 1.23×10^{-7} to 1.50×10^{-7} $kg.m^{-2}.s^{-1}$. By contrast, the fitted value of β was the same at both temperatures. The main effect of temperature was therefore an upward displacement of the net uptake curve and a shift of the transition region towards lower CO_2 concentrations, rather than a change in the steepness of the sigmoidal response. The fitted values of g_{NET} represent the effective net behavior of the complete LW system after subtraction of the OFF reference. They should therefore be interpreted as system-level fluxes under the investigated chamber, canopy, lighting, irrigation, and temperature conditions, rather than as direct measurements of the physiological uptake of individual leaves.

4.2. Pulse tests

Pulse tests were performed at 20 °C and 24 °C under three lighting conditions: LED switched OFF, LED at 50% (45 μmol m^{-2} s^{-1}), and LED at 100% (90 μmol m^{-2} s^{-1}). Figs. 7 and 8 report the normalized concentration $C^*(t)$ and the corresponding absolute concentration $C(t)$ for the two investigated temperatures. In both figures, curves OFF 1 and OFF 2 correspond to 20 °C, and curve OFF 3 to 24 °C. In detail, the final values of the OFF 1, 2, and 3 tests were 1493 ppm, 1502 ppm, and 1519 ppm, respectively, corresponding to a maximum variation of approximately 2%. The effect of temperature on the OFF reference was therefore negligible compared with the differences observed under illumination.

At 20 °C, the ON curves remained below the OFF reference throughout the tests, and the separation increased progressively with time. At 50% LED intensity, the three final concentrations ranged from 1242ppm to 1330ppm. Although their initial concentrations $C(0)$ were not identical, the variability in the corresponding concentration increase ΔC was approximately 5%, confirming good repeatability. Relative to the OFF condition, the final CO_2 increase was reduced by approximately 20% to 27%. At full illumination, the final concentrations decreased further to between 1115ppm and 1171ppm, with a variability in ΔC of approximately 4%. The corresponding reduction relative to OFF ranged from 35%to 39%.

A similar response was observed at 24 °C. At 50% LED intensity, the final concentrations were 1244ppm, 1242ppm, and 1253ppm. Since $C(0)$ was approximately 510ppm for the three tests, ΔC ranged only from 732ppm to 740ppm, corresponding to a variation of approximately

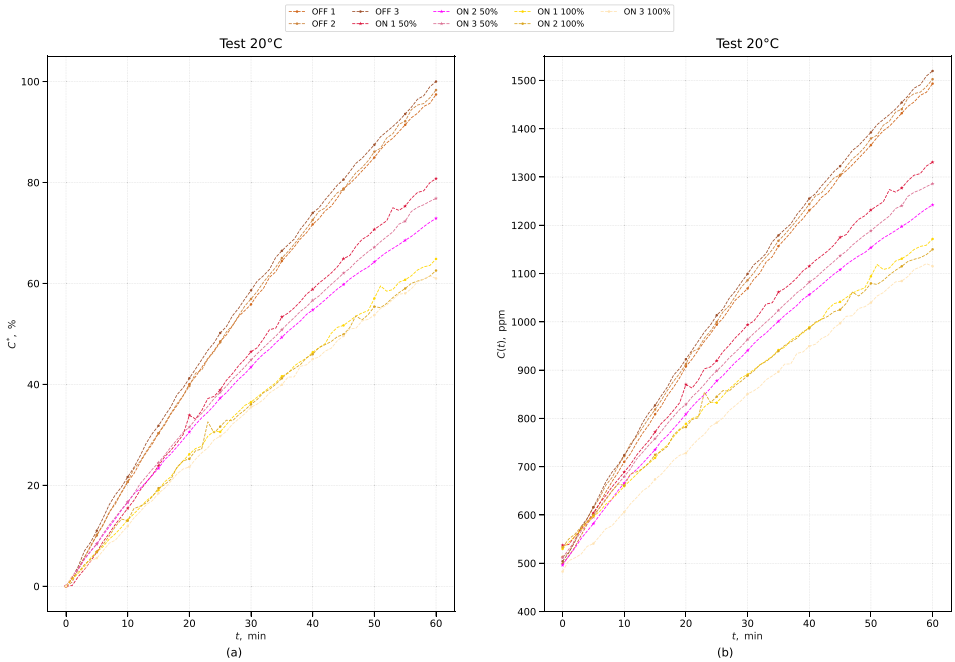

Fig. 7. Pulse-type tests performed at 20 °C. Panel (a) reports the normalized CO_2 concentration $C^*(t)$, whereas panel (b) shows the absolute concentration $C(t)$ in ppm.

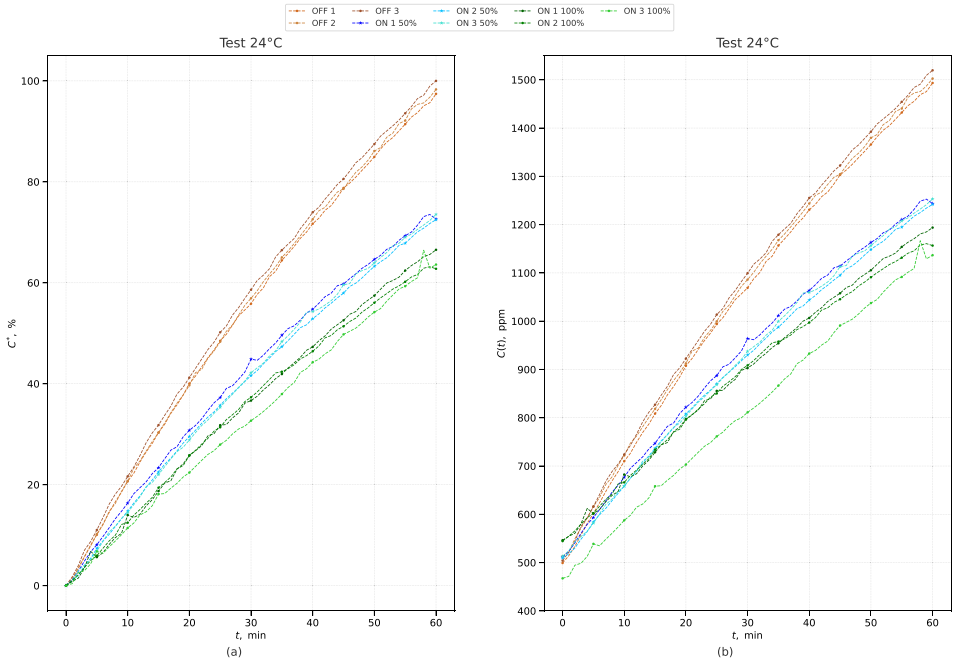

Fig. 8. Pulse-type tests performed at 24 °C. Panel (a) reports the normalized CO_2 concentration $C^*(t)$, whereas panel (b) shows the absolute concentration $C(t)$ in ppm.

1.15%. The final CO_2 increase was 26% to 27% lower than in the OFF condition. At 100% LED intensity, the final concentrations ranged from 1137ppm to 1194ppm, and the reduction relative to OFF was approximately 33% to 37%.

Overall, increasing the LED intensity from 50% to 100% consistently reduced CO_2 accumulation at both temperatures. By contrast, the influence of temperature was more limited: at 50% illumination, the results at 24 °C showed a slightly greater and more repeatable reduction, whereas the two temperatures produced comparable results under full illumination.

The same behavior can be expressed in terms of equivalent occupants, as reported in Table 7. Under OFF conditions, the mean CO_2 increase over each 10 min interval was 162 ppm to 165 ppmppm, corresponding to approximately 3.3 equivalent occupants aged 6–11 years engaged in school activities at 1.3met, as defined in Section 3.2. At 50% LED intensity, the mean increase was 128ppm at 20 °C and 123ppm at 24 °C, corresponding to approximately 2.6 and 2.5 equivalent occupants, respectively. When calculated relative to the corresponding OFF reference, these values represent reductions of approximately 21% at 20 °C and 25% at 24 °C. At full illumination, a reduction of about 35%

Table 7
Equivalent simulated occupants as a function of lighting conditions and temperature.

Lighting (%)	T (°C)	Mean ΔC (ppm/10 min, 3 tests)	Equivalent simulated occupants	Reduction vs. OFF (%)
OFF, 0	20	162	3.3	
OFF, 0	24	165	3.3	
ON, 50	20	128	2.6	21
ON, 50	24	123	2.5	25
ON, 100	20	105	2.1	35
ON, 100	24	107	2.1	35

Table 8
Integrated CO_2 pulse area M and efficiency η as a function of temperature and LED intensity.

T(°C)	LED(%)	Test	M(ppm min)	η(-)
OFF reference			33,990	
20	50	1	28,551	0.16
		2	26,950	0.21
		3	25,385	0.25
		Avg.	26,962	0.21
	100	1	23,043	0.32
		2	22,861	0.33
		3	20,214	0.41
		Avg.	22,040	0.35
24	50	1	26,043	0.23
		2	25,390	0.25
		3	25,039	0.26
		Avg.	25,491	0.25
	100	1	23,869	0.30
		2	23,560	0.31
		3	19,188	0.44
		Avg.	22,206	0.35

was found at both temperatures. Under the assumed emission and activity conditions, the reduction obtained at full illumination was therefore equivalent to offsetting approximately the CO_2 contribution of one child.

The integrated pulse areas reported in Table 8 confirm the trends observed in the concentration profiles. As indicated by the values of η, LED intensity had the clearest influence on pulse-test performance, whereas the temperature effect depended on the lighting level and became negligible at full illumination. Overall, the lower final concentration increase, reduced equivalent occupancy, and smaller integrated exposure consistently demonstrate the ability of the illuminated LWs to limit CO_2 accumulation under repeated indoor emission pulses.

5. Conclusions

This study quantified the ability of passive living walls (LWs) to mitigate indoor CO_2 concentrations through decay and pulse tests performed in a full-scale climate chamber. Illumination increased the decay constant, shortened the half-decay time, and reduced cumulative CO_2 exposure. The best decay performance was observed at 24 °C, consistent with the higher net uptake predicted by the fitted $g_{NET}(C)$ relationship. After subtraction of the OFF reference contribution, which takes into account the residual air exchange and other background effects, the net LW-equivalent CO_2 removal airflow rate was found to be 5.75 $m^3\ h^{-1}$ at 20 °C and 12.39 $m^3\ h^{-1}$ at 24 °C.

The pulse tests confirmed that the illuminated LWs limited CO_2 accumulation under repeated emissions simulating approximately three school-age children. After 60 min, the mean concentration increase was reduced by 20–27% and 35–39% at 20 °C under 50% and 100% LED intensity, respectively, and by 26–27% and 33–37% at 24 °C. Under full illumination, the equivalent respiratory load decreased from 3.3 to 2.1 occupants. LED intensity had the clearest influence, whereas the effect of temperature was moderate at reduced illumination and negligible at full illumination.

The experiments were conducted at two fixed temperature setpoints, selected as representative of classroom conditions during winter and intermediate seasons. Real buildings, however, are characterized by fluctuating temperature, humidity, lighting, occupancy, and ventilation, and the observed performance should therefore be validated under dynamic in situ conditions. The net LW contribution was limited but non-negligible, remaining below the EN 16,798–1 design airflow requirements. Passive LWs should consequently be regarded as complementary biological sinks rather than substitutes for ventilation. Larger or optimized systems may provide greater mitigation, including in more densely occupied spaces, but their performance cannot be assumed to increase linearly with vegetated area and requires specific experimental validation.

Future work should include long-term tests in real buildings and the implementation of $g_{NET}(C)$ as a biological sink term in dynamic IAQ and building-energy simulations. The potential reduction in ventilation energy should be assessed together with LED electricity use, irrigation demand, and lighting-related cooling loads through a dedicated thermo-economic and net energy benefit analysis.

CRediT authorship contribution statement

Gianluca Coccia: Writing – review & editing, Writing – original draft, Supervision, Methodology, Conceptualization. **Feliciano Falcone:** Writing – original draft, Validation, Investigation, Data curation. **Luca Tarabelli:** Validation, Investigation. **Costanzo Di Perna:** Supervision, Resources. **Elisa Di Giuseppe:** Writing – review & editing, Methodology. **Marco D'Orazio:** Writing – review & editing, Supervision, Project administration, Funding acquisition.

Declaration of competing interest

The authors declare that they have no known competing financial interests or personal relationships that could have appeared to influence the work reported in this paper.

Acknowledgements

This research belongs to the project NEUROPLANT (P2022MNX4 S), "The development of an artificial intelligence tool to predict phytoremediation of indoor air, through NEURal netwOrks trained with measurements of pollutant removal by PLANTs and their associated microbiome at different spatial and temporal scale", which was funded by the PRIN PNRR 2022 program of the Italian Ministry of University and Research (MUR).

The authors would like to thank Pellegrini Giardini, and in particular Dr. A. Pellegrini and P. Curini, for providing the plant species used in the living walls, together with part of the experimental equipment, and for their valuable support throughout the experimental campaign. The authors also thank the laboratory technician F. Tartaglini for his support during the installation of the experimental setup.

Data availability

Data will be made available upon request.

References

[1] G. Chiesa, M. Vigliotti, Comparing mechanical ventilation control strategies for indoor air quality: monitoring and simulation results of a school building in Northern Italy, Energy Build. 322 (2024), https://doi.org/10.1016/j.enbuild.2024.114665
[2] N.E. Klepeis, W.C. Nelson, W.R. Ott, J.P. Robinson, A.M. Tsang, P. Switzer, J.V. Behar, S.C. Hern, W.H. Engelmann, The national human activity pattern survey (NHAPS): a resource for assessing exposure to environmental pollutants, Journal of Exposure Analysis and Environmental Epidemiology 11 (2001) 231–252.
[3] T.M. Mata, A.A. Martins, C.S. Calheiros, F. Villanueva, N.P. Alonso-Cuevilla, M.F. Gabriel, G.V. Silva, Indoor air quality: a review of cleaning technologies, Environments 9 (9) (2022), https://doi.org/10.3390/environments9090118

[4] M.D.P. Navarrete-Meneses, C. Salas-Labadía, F. Gómez-Chávez, P. Pérez-Vera, Environmental pollution and risk of childhood cancer: a scoping review of evidence from the last decade, Int. J. Mol. Sci. 25 (6) (2024), https://doi.org/10.3390/ijms25063284

[5] J. Hu, Y. He, X. Hao, N. Li, Y. Su, H. Qu, Optimal temperature ranges considering gender differences in thermal comfort, work performance, and sick building syndrome: a winter field study in university classrooms, Energy Build. 254 (2022), https://doi.org/10.1016/j.enbuild.2021.111554

[6] R. Sivarethinamohan, S. Sujatha, S. Priya, Sankaran, A. Gafoor, Z. Rahman, Impact of air pollution in health and socio-economic aspects: review on future approach, in: Materials Today: Proceedings, 37, Elsevier Ltd, 2020, pp. 2725–2729, https://doi.org/10.1016/j.matpr.2020.08.540

[7] D. Etheridge, M. Sandberg, Building Ventilation: Theory and Measurement, Wiley, Chichester, 1996.

[8] D. Maier, Perspective of using green walls to achieve better energy efficiency levels. A bibliometric review of the literature, Energy Build. 264 (2022), https://doi.org/10.1016/j.enbuild.2022.112070

[9] A.K. Persily, Field measurement of ventilation rates, Indoor Air 26 (2016) 97–111.

[10] G. Hutton, E. Rehfuess, F. Tediosi, Evaluation of the costs and benefits of interventions to reduce indoor air pollution, Energy Sustain. Dev. 11 (2007) 34–43, https://doi.org/10.1016/S0973-0826(08)60408-1

[11] M.A. Gonzalez-Meler, L. Taneva, R.J. Trueman, Plant respiration and elevated atmospheric CO_2 concentration: cellular responses and global significance, Ann. Bot. 94 (5) (2004) 647–656, https://doi.org/10.1093/aob/mch189

[12] G. Boulanger, T. Bayeux, C. Mandin, S. Kirchner, B. Vergriette, V. Pernelet-Joly, P. Kopp, Socio-economic costs of indoor air pollution: a tentative estimation for some pollutants of health interest in France, Environ. Int. 104 (2017) 14–24, https://doi.org/10.1016/j.envint.2017.03.025

[13] C.E. Cox, S.S. Carson, J.A. Govert, L. Chelluri, G.D. Sanders, An economic evaluation of prolonged mechanical ventilation, Crit. Care Med. 35 (2007) 1918–1927, https://doi.org/10.1097/01.CCM.0000275391.35834.10

[14] W. Yao, X. Zhang, Q. Gong, The effect of exposure to the natural environment on stress reduction: a meta-analysis, Urban For. Urban Green. 57 (2021), https://doi.org/10.1016/j.ufug.2020.126932

[15] M. Radić, M.B. Dodig, T. Auer, Green facades and living walls-a review establishing the classification of construction types and mapping the benefits, Sustainability 11 (17) (2019), https://doi.org/10.3390/su11174579

[16] L. Dominici, R. Fleck, R.L. Gill, T.J. Pettit, P.J. Irga, E. Comino, F.R. Torpy, Analysis of lighting conditions of indoor living walls: effects on CO_2 removal, J. Build. Eng. 44 (2021), https://doi.org/10.1016/j.jobe.2021.102961

[17] M. Manso, J. Castro-Gomes, Green wall systems: a review of their characteristics, Renew. Sustain. Energy Rev. 41 (2015) 863–871, https://doi.org/10.1016/j.rser.2014.07.203

[18] M. Manso, I. Teotónio, C.M. Silva, C.O. Cruz, Green roof and green wall benefits and costs: a review of the quantitative evidence, Renew. Sustain. Energy Rev. 135 (2021), https://doi.org/10.1016/j.rser.2020.110111

[19] M. Köhler, Green facades-a view back and some visions, Urban Ecosyst. 11 (2008) 423–436, https://doi.org/10.1007/s11252-008-0063-x

[20] P. Kio, A.K. Ali, In situ experimental evaluation of a novel modular living wall system for industrial symbiosis, Energy Build. 252 (2021), https://doi.org/10.1016/j.enbuild.2021.111405

[21] T. Liberalesso, C. Oliveira Cruz, C. Matos Silva, M. Manso, Green infrastructure and public policies: an international review of green roofs and green walls incentives, Land Use Policy 96 (2020), https://doi.org/10.1016/j.landusepol.2020.104693

[22] P.J. Irga, T.J. Pettit, F.R. Torpy, The phytoremediation of indoor air pollution: a review on the technology development from the potted plant through to functional green wall biofilters, Rev. Environ. Sci. Bio/Technol. 17 (2018) 395–415, https://doi.org/10.1007/s11157-018-9465-2

[23] K. Gunawardena, K. Steemers, Living walls in indoor environments, Build. Environ. 148 (2019) 478–487, https://doi.org/10.1016/j.buildenv.2018.11.014

[24] D.L. Jones, P. Hinsinger, The rhizosphere: complex by design, in: Plant and Soil, 312, 2008, pp. 1–6, https://doi.org/10.1007/s11104-008-9774-2

[25] K. Karimi, M. Farrokhzad, G. Roshan, M. Aghdasi, Evaluation of effects of a green wall as a sustainable approach on reducing energy use in temperate and humid areas, Energy Build. 262 (2022), https://doi.org/10.1016/j.enbuild.2022.112014

[26] F. Scamoni, C. Scrosati, M. Depalma, B. Barozzi, Experimental evaluations of acoustic properties and long-term analysis of a novel indoor living wall, J. Build. Eng. 47 (2022), https://doi.org/10.1016/j.jobe.2021.103890

[27] X. Ma, M. Du, P. Deng, T. Zhou, B. Hong, Effects of green walls on thermal perception and cognitive performance: an indoor study, Build. Environ. 250 (2024), https://doi.org/10.1016/j.buildenv.2024.111180

[28] P. Wang, W.T. Chong, Y.H. Wong, Y.C. Tan, T. Cui, J. Wu, Significance analysis and evaluation of the impact of a new sustainable ecosystem on the microenvironment of multi-level thermal humidity, J. Build. Eng. 97 (2024), https://doi.org/10.1016/j.jobe.2024.110872

[29] L. Wang, M.J. Witte, Integrating building energy simulation with a machine learning algorithm for evaluating indoor living walls' impacts on cooling energy use in commercial buildings, Energy Build. 272 (2022), https://doi.org/10.1016/j.enbuild.2022.112322

[30] X. Meng, L. Yan, F. Liu, A new method to improve indoor environment: combining the living wall with air-conditioning, Build. Environ. 216 (2022), https://doi.org/10.1016/j.buildenv.2022.108981

[31] D. Zhang, L. Zhang, Y. Zhang, Investigation of the indoor CO_2 removal efficiency and fresh air energy savings of living walls in office spaces, J. Build. Eng. 90 (2024), https://doi.org/10.1016/j.jobe.2024.109422

[32] Y. Yungstein, D. Helman, Cooling, CO_2 reduction, and energy-saving benefits of a green-living wall in an actual workplace, Build. Environ. 236 (2023), https://doi.org/10.1016/j.buildenv.2023.110220

[33] K. Gillis, B. Gatersleben, A review of psychological literature on the health and wellbeing benefits of biophilic design, Buildings 5 (2015) 948–963.

[34] D. Tudiwer, A. Korjenic, The effect of an indoor living wall system on humidity, mould spores and CO_2-concentration, Energy Build. 146 (2017) 73–86, https://doi.org/10.1016/j.enbuild.2017.04.048

[35] I. Danielski, A. Svensson, K. Weimer, L. Lorentzen, M. Warne, Effects of green plants on the indoor environment and wellbeing in classrooms—a case study in a Swedish school, Sustain. (Switz.) 14 (2022), https://doi.org/10.3390/su14073777

[36] F.R. Torpy, P.J. Irga, M.D. Burchett, Profiling indoor plants for the amelioration of high CO_2 concentrations, Urban Forestry and Urban Greening 13 (2014) 227–233, https://doi.org/10.1016/j.ufug.2013.12.004

[37] E. van Tongerlo, G. Trouwborst, S.W. Hogewoning, W. van Ieperen, J.A. Dieleman, L.F. Marcelis, Crassulacean acid metabolism species differ in the contribution of C3 and C4 carboxylation to end of day CO_2 fixation, Physiologia Plantarum 172 (2021) 134–145, https://doi.org/10.1111/ppl.13312

[38] F. Torpy, M. Zavattaro, P. Irga, Green wall technology for the phytoremediation of indoor air: a system for the reduction of high CO_2 concentrations, Air Quality, Atmosphere and Health 10 (2017) 575–585, https://doi.org/10.1007/s11869-016-0452-x

[39] V. Hörmann, K.-R. Brenske, C. Ulrichs, Suitability of test chambers for analyzing air pollutant removal by plants and assessing potential indoor air purification, Water Air Soil Pollut. 228 (2017) 402.

[40] V. Hörmann, K.-R. Brenske, C. Ulrichs, Assessment of filtration efficiency and physiological responses of selected plant species to indoor air pollutants (toluene and 2-ethylhexanol) under chamber conditions, Environ. Sci. Pollut. Res. 25 (2018) 447–458.

[41] I. Parseh, H. Teiri, Y. Hajizadeh, K. Ebrahimpour, Phytoremediation of benzene vapors from indoor air by schefflera arboricola and spathiphyllum wallisii plants, Atmos. Pollut. Res. 9 (2018) 1083–1087.

[42] W. Sriprapat, P. Thiravetyan, Efficacy of ornamental plants for benzene removal from contaminated air and water: effect of plant associated bacteria, International Biodeterioration & Biodegradation 113 (2016) 262–268.

[43] A. Aydogan, L.D. Montoya, Formaldehyde removal by common indoor plant species and various growing media, Atmos. Environ. 45 (2011) 2675–2682, https://doi.org/10.1016/j.atmosenv.2011.02.062

[44] C. Treesubsuntorn, P. Thiravetyan, Removal of benzene from indoor air by dracaena sanderiana: effect of wax and stomata, Atmos. Environ. 57 (2012) 317–321.

[45] A. Tani, C.N. Hewitt, Uptake of aldehydes and ketones at typical indoor concentrations by houseplants, Environ. Sci. Technol. 43 (2009) 8338–8343.

[46] A. Setsungnern, C. Treesubsuntorn, P. Thiravetyan, The influence of different light quality and benzene on gene expression and benzene degradation of chlorophytum comosum, Plant Physiology and Biochemistry 120 (2017) 95–102.

[47] M.M.S. Shamsuri, A.M. Leman, Indoor plants as a filtration of indoor air pollution: a review, Journal of Occupational Safety and Health 12 (2015).

[48] H. Teiri, H. Pourzamani, Y. Hajizadeh, Phytoremediation of VOCs from indoor air by ornamental potted plants: a pilot study using a palm species under the controlled environment, Chemosphere 197 (2018) 375–381.

[49] F. Torpy, N. Clements, M. Pollinger, A. Dengel, I. Mulvihill, C. He, P. Irga, Testing the single-pass VOC removal efficiency of an active green wall using methyl ethyl ketone (MEK), Air Quality, Atmosphere & Health 11 (2018) 163–170.

[50] Danoplus, DP-380 quantum PAR meter: instruction manual, 2023, https://www.danoplus.com/wp-content/uploads/2024/04/DP-380_Manual_EN.pdf.

[51] D.J. Watson, Comparative physiological studies on the growth of field crops: I. variation in net assimilation rate and leaf area between species and varieties, and within and between years, Ann. Bot. 11 (1947) 41–76, https://doi.org/10.1093/oxfordjournals.aob.a083148

[52] H. Fang, F. Baret, S. Plummer, G. Schaepman-Strub, An overview of global leaf area index (LAI): methods, products, validation, and applications, Rev. Geophys. 57 (3) (2019) 739–799, https://doi.org/10.1029/2018RG000608

[53] N.J. Bréda, Ground-based measurements of leaf area index: a review of methods, instruments and current controversies, J. Exp. Bot. 54 (392) (2003) 2403–2417, https://doi.org/10.1093/jxb/erg263

[54] I. Jonckheere, S. Fleck, K. Nackaerts, B. Muys, P. Coppin, M. Weiss, F. Baret, Review of methods for in situ leaf area index determination Part I. theories, sensors and hemispherical photography, Agric. for. Meteorol. 121 (2004) 19–35, https://doi.org/10.1016/j.agrformet.2003.08.027

[55] R. Bakhshoodeh, C. Ocampo, C. Oldham, Evapotranspiration rates and evapotranspirative cooling of green façades under different irrigation scenarios, Energy Build. 270 (2022), https://doi.org/10.1016/j.enbuild.2022.112223

[56] F. Convertino, G. Vox, E. Schettini, Evaluation of the cooling effect provided by a green façade as nature-based system for buildings, Build. Environ. 203 (2021), https://doi.org/10.1016/j.buildenv.2021.108099

[57] A. De Bock, B. Belmans, S. Vanlanduit, J. Blom, A.A. Alvarado-Alvarado, A. Audenaert, A review on the leaf area index (LAI) in vertical greening systems, Build. Environ. 229 (2023), https://doi.org/10.1016/j.buildenv.2022.109926

[58] A. Wang, J. Lv, J. Wang, K. Shi, CO_2 enrichment in greenhouse production: towards a sustainable approach, Front. Plant Sci. 13 (2022), https://doi.org/10.3389/fpls.2022.1029901

[59] Y. Li, G.M. Leung, J.W. Tang, X. Yang, C.Y. Chao, J.Z. Lin, J.W. Lu, P.V. Nielsen, J. Niu, H. Qian, A.C. Sleigh, H.J. Su, J. Sundell, T.W. Wong, P.L. Yuen, Role of ventilation in airborne transmission of infectious agents in the built environment - a multidisciplinary systematic review, Indoor Air 17 (1) (2007) 2–18, https://doi.org/10.1111/j.1600-0668.2006.00445.x

[60] Z. Jiang, T. Kobayashi, T. Yamanaka, M. Sandberg, A literature review of cross ventilation in buildings, Energy Build. 291 (2023), https://doi.org/10.1016/j.enbuild.2023.113143
[61] D.W. Etheridge, Unsteady flow effects due to fluctuating wind pressures in natural ventilation design—mean flow rates, Build. Environ. 35 (2000) 111–133.
[62] N. Izadyar, W. Miller, Ventilation strategies and design impacts on indoor airborne transmission: a review, Build. Environ. 218 (2022), https://doi.org/10.1016/j.buildenv.2022.109158
[63] D. Etheridge, Natural ventilation of buildings theory measurement and design, Int. J. Vent. 10 (4) (2012) 405–406, https://doi.org/10.1080/14733315.2012.11683965
[64] R. Killick, P. Fearnhead, I.A. Eckley, Optimal detection of changepoints with a linear computational cost, J. Am. Stat. Assoc. 107 (2012) 1590–1598.
[65] S.C. Chapra, R.P. Canale, Numerical Methods for Engineers, McGraw-Hill Education, 2015.
[66] R.J. Tallarida, R.B. Murray, Area under a curve: trapezoidal and simpson's rules, in: Manual of Pharmacologic Calculations: With Computer Programs, Springer, 1987, pp. 77–81.
[67] S. Devi, N. Gupta, Dynamics of carbon dioxide gas (CO_2): effects of varying capability of plants to absorb CO_2, Nat. Resour. Model. 32 (2019), https://doi.org/10.1111/nrm.12174
[68] H. Agra, D. Uni, R. Horwitz, T. Klein, L. Blaustein, Leaf color segmentation and pot volume influence on the CO_2 absorption efficiency in two common green-wall plants, J. Green Build. 16 (2021), http://meridian.allenpress.com/jgb/article-pdf/16/3/3/2904127/i1943-4618-16-3-3.pdf.
[69] N.H. Weerasinghe, P.K. Silva, R.R. Jayasinghe, W.P. Abeyrathna, G.K.P. John, R.U. Halwatura, Reducing CO_2 level in the indoor urban built environment: analysing indoor plants under different light levels, Clean. Eng. Technol. 14 (2023), https://doi.org/10.1016/j.clet.2023.100645
[70] M. Jozay, H. Zarei, S. Khorasaninejad, T. Miri, Maximising CO_2 sequestration in the city: the role of green walls in sustainable urban development, Pollutants 4 (1) (2024) 91–116, https://doi.org/10.3390/pollutants4010007
[71] European Committee for Standardization, EN 16798-1:2019. Energy Performance of Buildings – Ventilation for Buildings – Indoor Environmental Input Parameters for Design and Assessment of Energy Performance of Buildings Addressing Indoor Air Quality, Thermal Environment, Lighting and Acoustics, Technical Report, CEN (European Committee for Standardization), Brussels, 2019.
[72] A. Persily, L. de Jonge, Carbon dioxide generation rates for building occupants, Indoor Air 27 (2017) 868–879, https://doi.org/10.1111/ina.12383
[73] ASHRAE, ANSI/ASHRAE standard 62.1-2025, ventilation and acceptable indoor air quality, 2025, https://www.ashrae.org/technical-resources/bookstore/standards-62-1-62-2.
[74] International Organization for Standardization (ISO), ISO 16000-26:2012 - indoor air — Part 26: Sampling strategy for carbon dioxide (CO_2), 2012, https://www.iso.org/standard/52140.html.
[75] ASTM, ASTM D6245-18: standard guide for using indoor carbon dioxide concentrations to evaluate indoor air quality and ventilation, 2018, https://store.astm.org/d6245-18.html.
[76] B.E. Ainsworth, The Compendium of Physical Activities Tracking Guide, University of South Carolina, 2002.